Models of triplet self-trapped excitons in SiO_2, HfO_2, and $HfSiO_4$

D. Muñoz Ramo,[1,2] P. V. Sushko,[2,3] and A. L. Shluger[2,3]

[1]*Department of Earth Sciences, University College London, Gower Street, London WC1E 6BT, United Kingdom*

[2]*Department of Physics and Astronomy and the London Centre for Nanotechnology, University College London, Gower Street, London WC1E 6BT, United Kingdom*

[3]*WPI-Advanced Institute for Materials Research, Tohoku University, 2-1-1 Katahira, Aoba, Sendai, 980-8577 Japan*

(Received 2 September 2011; revised manuscript received 11 January 2012; published 30 January 2012)

We predict by means of density functional theory simulations the structures of self-trapped triplet excitons in HfO_2 and $HfSiO_4$, and compare their properties to those of the self-trapped exciton in α quartz. The character of the hole and electron localization in excitons strongly depends on the geometrical structure and dielectric properties of these materials. In HfO_2, the electron is localized predominantly on one Hf atom while the hole is localized on one or two oxygen atoms at the nearest or next-nearest-neighbor sites, depending on the crystal phase. We predict two exciton configurations in $HfSiO_4$ with the excited electron localized either on a Hf or on a Si atom and the hole localized on the nearest-neighbor oxygen atoms. Excitation and luminescence energies are calculated for all triplet exciton states and compared with the available experimental data.

DOI: 10.1103/PhysRevB.85.024120 PACS number(s): 61.72.Bb, 71.20.−b, 71.35.Aa

I. INTRODUCTION

Excitons are neutral quasiparticles in the form of electron-hole pairs, which propagate in a nonmetallic solid. They drastically alter the optical, magnetic as well as energy and charge transport properties of solids. In some insulating crystals excitons may become self-trapped and form small-radius states, which resemble an excited atom or molecule.[1] Self-trapping is caused by exciton-phonon interaction and is often accompanied by considerable local lattice distortion. Self-trapped excitons (STEs) can decay radiatively, yielding a distinctive luminescence, or nonradiatively, producing heat, transferring energy to impurities, or forming lattice defects. Radiation damage and scintillating properties are, thus, common motivations for studying STEs in nominally pure as well as in doped insulators.[1,2]

The existence of STEs has so far been firmly established only in a relatively small number of insulating materials, such as alkali and alkaline-earth halides, silica, rare-gas solids, perovskite-structured halides of the MgF_3 family and in some complex oxides.[1–4] However, experimental determination of detailed atomistic models of STEs has not been successful even for alkali halides, which are traditionally regarded as archetypal insulating materials, and in which the structure of STE and the dynamics of self-trapping processes have been studied most extensively.[1]

Theoretical studies of the structure and properties of self-trapped excitons also have a long history. Phenomenological theories[5] produced general criteria for self-trapping of excitons and suggested qualitative models of their structures.[6] However, they cannot provide detailed information concerning the electronic and atomic structures of STEs, which would enable full comparison of the theoretical predictions with experimental data.

Such atomistic models can be provided by quantum-mechanical calculations, as reviewed in Refs. 1, 2, 7, and 8. The early Hartree-Fock-type calculations predicted spectroscopic properties of STEs in alkali halides and in α-quartz in good agreement with experiment.[8,9] These calculations also emphasized the importance of accounting for the electron correlation in modeling STEs.[10] Initially, it has been expected that the electron correlation could be accounted for through the use of the density functional theory (DFT), but these hopes were soon dashed when it became clear that the self-interaction error, inherent in LDA and GGA functionals, prevents electron and hole localization and underestimates band gaps (see, for example, discussion in Ref. 11). Since then, several methods, such as hybrid density functionals with different amounts of the Hartree-Fock exchange and more accurate techniques using GW and other approaches (see, for example, Refs. 12–15), have been used to model polaron and exciton localization and self-trapping as well as for predicting the exciton spectra and structure in insulators.

Here, we revisit STE in α-quartz and predict the structures and study the properties of STEs in HfO_2 and $HfSiO_4$, which were recently employed in CMOS devices. Considering these three systems provides a unique perspective at how the structure and properties of STE in oxides depend on the crystalline structure.

The STE in α-quartz has been studied extensively both experimentally and theoretically.[1,2,14,16,17] Yet, the details of its atomic structure still remain controversial particularly due to the small size of clusters and periodic cells used in the simulations, which are known to constrain the exciton-induced lattice deformation.

Concerning the two other materials, there have been several suggestions that a photo-luminescence observed in monoclinic HfO_2 films is due to STE,[18,19] contradicted by the results of other experiments.[20] Since unambiguously detecting STEs in a material and determining their properties experimentally is extremely challenging,[1] theoretical calculations can provide guidance and aid their identification. In particular, it has been recently predicted theoretically that both electrons and holes can self-trap forming small-radius polarons in the monoclinic phase of HfO_2.[21] According to the phenomenological theory,[5] this is a strong indication that excitons can also self-trap in this material. Three stable phases (monoclinic, tetragonal, and cubic) of HfO_2 have different dielectric tensors[22] and, according to the same theory,[5,6] one

can expect that STEs can have different structures in different phases.

$HfSiO_4$ is the simplest representative of hafnium silicates ($Hf_xSi_{1-x}O_4$), which are used as gate oxides and are still poorly studied. The crystalline structure of $HfSiO_4$ has elements of both HfO_2 and SiO_2, which makes it an interesting material to consider, especially because STE is known to exist in α-quartz.[1] While we are not aware of any experimental studies of STE in $HfSiO_4$, intrinsic luminescence in a similarly structured Be_2SiO_4 has recently been attributed to STE.[23] We note that many properties of HfO_2 and $HfSiO_4$ are close to those of ZrO_2 and $ZrSiO_4$ and some of our results can be useful for understanding the properties of these and other, more complex oxides, which exhibit luminescence attributed to STE (see, e.g., Refs. 3 and 4).

This paper is organized as follows. In Sec. II, we describe the details of the models and methods used for our electronic structure calculations. The electronic structure of SiO_2 (α quartz), HfO_2 (in the cubic, tetragonal, and monoclinic phases), and $HfSiO_4$ is described in Sec. III. The results concerning exciton self-trapping in these three materials are presented in Sec. IV. Finally, our conclusions are presented in Sec. V.

II. COMPUTATIONAL DETAILS

Recently, there has been significant progress in developing efficient computational techniques for calculating electronic excitation spectra in wide band gap materials. Some of these techniques are based on using periodic DFT for the ground state and then applying Hedin's GW approximation and other methods (see, for example, Refs. 14, 15, and 24) to model excited states. However, modeling self-trapped excitons and exciton decomposition requires using large supercells and minimizing forces in excited states. Such calculations are still computationally challenging and rare.[14,17]

In this work, we study only the lowest energy triplet excitons, which is prompted by the experimental evidence[1,2] that this is indeed the lowest state of STE in alkali halides, alkali earth fluorides, α quartz, and other insulators. This approximation has been employed successfully in previous calculations of STEs, as discussed in, for example, Refs. 7–10. However, unlike in those studies, we use DFT and a nonlocal density functional. We note that the choice of the functional can be crucial for polaron and exciton description (see, e.g., Refs. 25 and 26). As shown below, in all cases considered in this paper, we predict the STE localization, but the calculated spectroscopic characteristics of STEs can be affected by the choice of the density functional.

We use two complementary computational schemes implementing periodic and embedded cluster methods. In both of them, a configuration of a triplet exciton is found by minimizing the total energy of a system with respect to the atomic positions and then the exciton luminescence energy is calculated. In addition, the optical transition energies for STE in monoclinic HfO_2 are calculated in an embedded cluster model using the time-dependent (TD)-DFT method implemented in the GAUSSIAN03 package.[27]

A. Periodic calculations

Periodic DFT calculations were performed with the CRYSTAL06 package,[28] which uses local basis sets of Gaussian-type orbitals (GTOs), and the hybrid B3LYP functional.[29,30] This functional has been used to predict defect and polaron properties in monoclinic HfO_2,[21,31,32] crystalline and amorphous SiO_2,[33–35] and in other insulators.[36,37]

The basis set for oxygen includes $14s$, $6p$, and $1d$ functions contracted to $1s$, $3sp$, and $1d$ shells using a $8/411/1$ scheme. For Si, the basis set includes $20s$, $12p$, and $1d$ functions contracted to $1s$, $3sp$, and $1d$ shells with a $8/831/1$ scheme. For Hf atoms, we used a relativistic effective core potential (RECP), which replaces all but 12 valence electrons. This RECP has been introduced by Stevens *et al.*[38] and adapted for the CRYSTAL code.[31] The Hf basis set consists of $6s$, $6p$, and $4d$ functions contracted to $3sp$ and $2d$ shells using a $411/31$ scheme.

The calculations of HfO_2 and $HfSiO_4$ were carried out using 96-atom supercells, constructed as $2 \times 2 \times 2$ and $2 \times 2 \times 1$ expansions of the HfO_2 and $HfSiO_4$ unit cells, respectively. In the case of α quartz, we used a 72-atom $2 \times 2 \times 2$ supercell. A Monkhorst-Pack mesh of nine k points in the irreducible part of the Brillouin zone was used for integration in the reciprocal space in all cases.

To facilitate initial hole and electron localization in the triplet state, we created small precursor distortions around particular lattice sites.[39,40] In particular, cations near a selected oxygen site have been displaced so as the Hf-O and Si-O bonds are elongated by $\sim$0.1 Å in both HfO_2 and $HfSiO_4$ and by $\sim$0.5 Å in SiO_2. The magnitude of the perturbation was selected on the basis of earlier calculations of the defect-induced atomic displacements in SiO_2 and HfO_2,[31,41] as it is expected to be sufficient for localizing both the hole and electron components of the exciton at an anion and some nearby cations, respectively.

B. Embedded cluster calculations for SiO_2

The structure of α–quartz was represented using a nearly spherical nanocluster. To construct it, we first optimized the geometrical structure of α-quartz using the periodic model and the CRYSTAL code. The infinite α-quartz lattice was then constructed from $Si(\frac{1}{2}O)_4$ tetrahedra. All such tetrahedra within 30 Å of a given oxygen site were attributed to the nanocluster and remaining ones were discarded. By construction,"halves" of the oxygen atoms ($\frac{1}{2}$O) remain only at the periphery of the nanocluster, while exactly two such halves of oxygen atoms occupy the same lattice site inside the nanocluster and therefore form a "full" oxygen atom. The ionic charges assigned to Si, O, and $\frac{1}{2}$O species relate as $Q{:}-Q/2{:}-Q/4$, where $Q = 2.4|e|$. By construction, the dipole moment of the nanocluster is negligibly small. Therefore as the size of the nanocluster increases, the electrostatic potential inside it converges up to a constant to that given by the Ewald summation of the infinite lattice.[42]

We used the $Si_8O_{25}Si^*_{18}$ quantum-mechanical (QM) cluster positioned at the center of the nanocluster. It includes two shells of Si and O atoms next to a central oxygen atom and is terminated by Si^* pseudoatoms described in detail

elsewhere.[41] The QM region is surrounded by a spherical shell in which Si and O ions are described using the classical shell model and interact with each other and with the QM atoms via the interatomic potentials[43] modified so as to reproduce the polarizability of oxygen ions. Finally, atoms in the remaining part of the nanocluster are treated as rigid ions and are kept fixed in their ideal bulk positions. They provide correct potential energy surface for both quantum and shell model atoms, which are allowed to relax in the course of the calculations. The QM contributions to the total energies and forces are calculated using the B3LYP density functional and standard Pople's 6-31G(d) basis set, which is comparable to that used in the periodic model calculations. To reduce the cost of the computations, oxygen atoms next to the interface region have been represented using a 6-31G basis set.

C. Embedded cluster calculations for m-HfO_2

Based on the relatively small radius of the lattice deformation induced by the STE in m-HfO_2, we used a simplified approach, where a quantum cluster including the STE and its vicinity was embedded in the rest of the crystal represented by a lattice of classical rigid ions.[31]

First, using a 96-atom supercell of m-HfO_2 as a building block, we constructed a nearly spherical nanocluster of the radius of ∼25 Å. The coordinates of ions in this supercell were preoptimized using the B3LYP functional and the CRYSTAL code. The classical ions of the nanocluster have been assigned charges of $+4|e|$ and $-2|e|$ for Hf and O, respectively. 15 Hf and 30 O atoms at the center of the nanocluster form a part of the system considered quantum mechanically and embedded into the electrostatic potential produced by the remaining part of the nanocluster. We represent classical Hf ions within 10 Å from the border of the QM cluster by large core pseudopotentials,[44] which substitute all but four outermost electrons. These atoms form an interface between the QM cluster and the classical environment and prevent artificial polarization of the electron density toward the positive point ions outside the QM cluster (see Ref. 31 for more details). We used the same GTO basis sets, pseudopotentials, and B3LYP density functional as in the periodic calculations.

To simulate the STE localized inside the QM cluster, positions of ions within 5 Å around the QM cluster center were made identical to those of the STE as obtained in the periodic model calculations. The displacements of ions induced by the STE beyond this distance are negligibly small.

In the case of $HfSiO_4$, the interface between the classical and the quantum regions includes both Hf and Si atoms. Creating such an embedding scheme is a complex task that goes beyond the aims of this study and we studied this material using only the periodic model.

III. DESCRIPTION OF THE LATTICES

In order to characterize the structure and electronic states of excitons in the three oxides considered in this work, we first briefly describe the differences in geometrical and electronic structures of these materials. A much more detailed description can be found in Refs. 45–47.

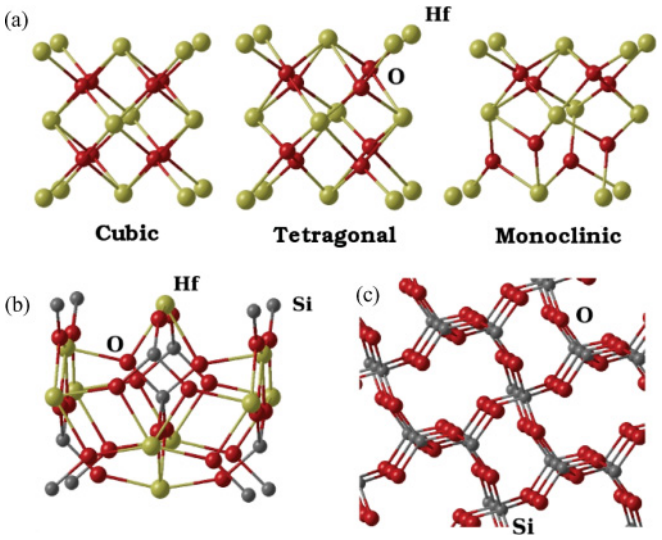

FIG. 1. (Color online) Geometrical structures of (a) cubic, tetragonal, and monoclinic HfO_2 (unit cells), (b) $HfSiO_4$ (unit cell), and (c) α-quartz SiO_2.

HfO_2 has three polymorphs at ambient pressure: a monoclinic phase (m-HfO_2), stable at temperatures below 2000 K, a tetragonal phase (t-HfO_2) stable between 2000 and 2870 K, and a cubic phase (c-HfO_2) stable at temperatures above 2870 K. Their geometric structures are shown in Fig. 1. Hf ions in m-HfO_2 are sevenfold coordinated by O ions and there are two oxygen sublattices: in one of them, oxygen ions are three coordinated and in the other, four coordinated by Hf ions. In the two other phases, there is only one oxygen sublattice with fourfold coordination and Hf atoms are eightfold coordinated.

The optimized lattice parameters along with the corresponding experimental values are summarized in Table I. The one-electron B3LYP band gaps for the cubic, tetragonal, and monoclinic phases are about 5.9, 6.5, and 6.1 eV, respectively. The value for the monoclinic phase agrees well with the experimental estimates of around 5.8 eV.[48,49] In all phases, the valence band is mainly composed of oxygen $2p$ states.

TABLE I. Lattice parameters calculated in this work using the B3LYP density functional. The corresponding experimental values have been obtained from Refs. 53 (HfO_2), 54 (SiO_2), and 55 ($HfSiO_4$).

Compound	Parameters	This work	Expt.
SiO_2 (α-quartz)	a (Å)	4.964	4.902
	c (Å)	5.469	5.400
	γ (deg)	120.0	120.0
m-HfO_2	a (Å)	5.153	5.119
	b (Å)	5.212	5.170
	c (Å)	5.314	5.298
	γ (deg)	99.47	99.18
t-HfO_2	a (Å)	5.076	5.06
	c (Å)	5.195	5.18
c-HfO_2	a (Å)	5.09	5.07
$HfSiO_4$	a (Å)	6.632	6.57
	c (Å)	6.046	5.97

The bottom of the conduction band is mostly composed of 5*d* states of hafnium, with some small contribution of oxygen 3*p* states. In the monoclinic phase, the contributions from the three-coordinated and four-coordinated oxygen ions are equally distributed in the whole of the valence band except for the states near the VBM: these states are exclusively composed of linear combinations of 2*p* states of three-coordinated oxygens.

$HfSiO_4$ is tetragonal at room temperature. Hf atoms are sevenfold coordinated and Si atoms are fourfold coordinated by oxygen atoms, whereas oxygen atoms are coordinated by two Hf atoms and one Si atom [see Fig. 1(b)]. The calculated band gap in this system is about 7.5 eV. While we are not aware of experimental reports of this band gap, the estimates for amorphous phases of $(HfO_2)_x(SiO_2)_{1-x}$ at different values of x suggest[50,51] that the band gap of crystalline $HfSiO_4$ can be between 6.5 and 7.0 eV. The top of the valence band is mainly composed of oxygen 2*p* states. The conduction band is formed from the Hf 5*d* states and Si 3*p* states with Hf states dominating the lower part of the conduction band up to about 3 eV above the CBM.

The α-quartz lattice is shown in Fig. 1(c). Each Si atom is fourfold coordinated by a pair of "long" (1.62 Å) and "short" (1.61 Å) bonds with oxygen atoms, while oxygen atoms are twofold coordinated. This lattice has lower atom number density than that of HfO_2 and large interstitial spaces. The calculated one-electron band gap of 9.2 eV is slightly larger than the experimental value of 8.9 eV.[52] The bottom of the conduction band is formed of Si 3*p* and 3*d* and O 3*p* states.

IV. STRUCTURE OF SELF-TRAPPED EXCITONS

Below we describe the results of the calculations, including the geometrical structures of relaxed STEs and changes in the one-electron densities of states, for the triplet excited state for each of the crystals. We also report the exciton excitation energies for vertical singlet-triplet transitions E_e the relaxation energies in the triplet state E_r and the photo-luminescence (PL) energies E_l.

The exciton excitation energies E_e are calculated using the ΔSCF method as differences between the total energies of a crystal in the perfect lattice configuration in the ground singlet and the lowest triplet states.

The exciton relaxation energy E_r is the difference between the energies of relaxed and unrelaxed lowest triplet states. In these calculations, the unrelaxed triplet state in the perfect lattice supercell represents the hole and electron states delocalized over sublattices forming the band edges in the particular material. For instance, in the case of $HfSiO_4$, the obtained solution had partial electron localization on Hf atoms of the lattice responsible for the bottom of the conduction band.

The photoluminescence energies correspond to the vertical triplet-singlet transition at the geometrical configuration of the relaxed triplet state and are calculated using the ΔSCF method as the difference between the total energy of the fully relaxed triplet state and the ground singlet state at the triplet geometric structure. We also used TD-DFT to calculate the photoluminescence energies and the optical absorption energies of the electron and hole components of STE in m-HfO_2 and α quartz within the embedded cluster method.

A. Exciton in α-quartz SiO_2

Electrons in α quartz can be excited via singlet-singlet transitions using different types of ionizing and optical radiation (see, for example, discussion in Ref. 56). These excitations are accompanied by a long-lived luminescence attributed to recombination of the electron and hole components of triplet STEs.[1,57] Since the recombination occurs via a spin-forbidden transition, the photoluminescence has lifetime of the order of milliseconds. While two luminescence energies of ~2.5 and ~2.7 eV have been reported, the assignment of the 2.5 eV band to the STE is not universal.[58,59]

The first attempt to predict theoretically a configuration and properties of the triplet STE in SiO_2 by quantum-mechanical methods used an idealized β-cristobalite structure and a cluster model and calculated the luminescence energy of 2.3 eV.[60] Subsequent *ab initio* calculations of α-quartz using periodic and cluster models and different theoretical methods reported qualitatively similar STE models and luminescence energies broadly in agreement with experiment[14,16,17] and have provided models of the spin localization and lattice distortion induced by the presence of the exciton state. In addition, periodic DFT calculations were carried out for excitons trapped in amorphous silica.[61]

The periodic model offers a better representation of the perfect lattice and, thus, is less biased an approach to predicting whether an exciton would self-trap in a particular crystal structure. Due to computational constrains, most of the previous calculations have been performed in supercells containing between 18 and 72 atoms. However, in the case of the small supercells, the lattice relaxation is not accounted for beyond the nearest neighbors. A deficiency of the earlier periodic calculations in relatively large cells is that these have been carried out at the LDA or GGA levels, which tend to exaggerate the spatial extend of both the hole and electronic components of the exciton. This could be one of the main reasons why the most common configuration of the STE was found to be unstable in the 72 atom unit cell calculation.[17]

1. Configurations of the STE in α-quartz

Using the B3LYP functional and both a 72-atom period cell and the embedded cluster model we obtained two STE configurations, denoted STE1 and STE2, shown in Fig. 2. They effectively correspond to breaking "long" and "short" Si-O bonds as a result of excitation. In the periodic calculation of the STE1, an electron is strongly localized at one Si (Si1) atom (73% localization according to the Mulliken population analysis), while the hole is predominantly localized at the nearest-neighbor O atom (O1). The exciton is also inducing spin polarization of six nearest-neighbor oxygen atoms seen in Fig. 2. This charge transfer excitation is accompanied by significant local lattice relaxation. In particular, the distance between the Si1 and O1 atoms increases by about 1.0 Å. At the same time, the length of the Si2-O1 bond is reduced by 0.05 Å only and its electronic structure remains unaffected. The distance between the two Si atoms bridged by O1 is increased by ~0.4 Å.

In the STE2, the hole is also at O1 but the electron is localized at Si2 (see Fig. 2). The local relaxation is, however, slightly different with the O1-Si2 distance increasing by about

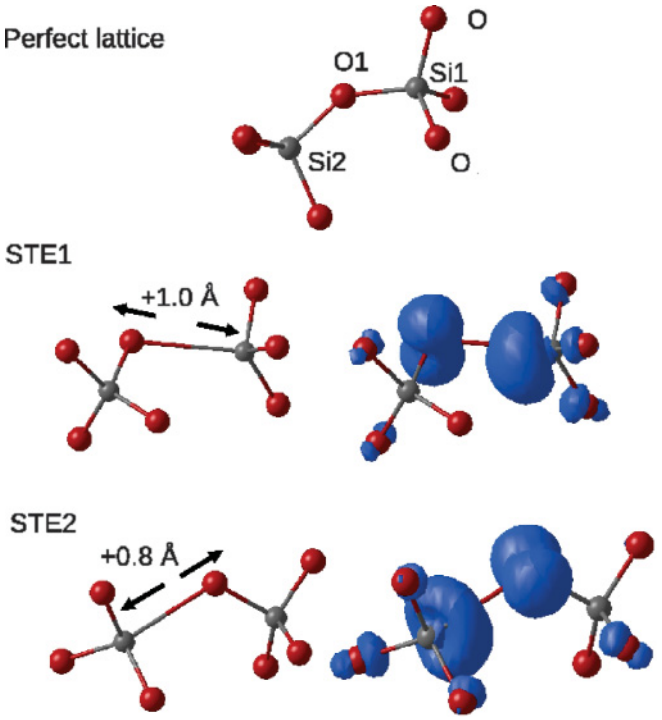

FIG. 2. (Color online) Schematic of the lattice relaxation and spin localization in the STE1 and STE2 configurations in SiO_2. Left part shows the lattice relaxation and right part shows the surface of the constant spin density with value S = 0.01. Bright and dark spheres represent Si and O atoms, respectively.

0.8 Å with respect to that in the ideal lattice. In periodic calculations, this configuration is by about 0.3 eV higher in energy than that of STE1. Assuming that a transition between the two STE configurations may take place adiabatically, we calculated the height of the transition barrier using a linear interpolation approach and found that the STE2-to-STE1 barrier is 1.5 eV, while the barrier for reverse transition is 1.8 eV.

The embedded cluster calculations predict a qualitatively similar exciton model. The geometric parameters of the local structure in both configurations are shown in Table II. In fully relaxed configurations, the Si-O bond lengths are nearly identical in the STE1 and STE2. However, the Si-O distances corresponding to the broken bonds differ by more than 0.2 Å and the Si-O-Si angles — by 7° from those in periodic calculations. The fully relaxed excitons are almost isoenergetic, with STE2 being by only 0.03 eV more stable than STE1.

Such large displacements of atoms in the first coordination shell of the STE drive strong distortions of the surrounding lattice. For both exciton configurations, atoms located within 3.5 Å from the STE site in periodic calculations displace, on average, by 0.3 Å, while other atoms of the supercell displace by 0.1 Å. However, a more detailed analysis of the lattice deformation (see Supplemental Material[62]) clearly demonstrates that the directions and values of displacements in periodic calculations are strongly affected by the interaction between periodically translated excitons in different cells. These interactions induce competing forces leading to, e.g.,

TABLE II. Comparison of the geometric parameters for quartz STE calculated in this work using the periodic and cluster models. Parameters in the table are silicon-oxygen distances (Si_k-O, $k = 1,2$) and silicon-oxygen-silicon angle $\theta(Si_1\text{-O-}Si_2)$ at the STE site. The distances are given in Å, the angles are in degrees.

		Si_1-O	Si_2-O	$\theta(Si_1\text{-O-}Si_2)$
Fully relaxed structure				
Periodic	STE1	1.67	2.61	106.4
Periodic	STE2	2.42	1.67	119.4
Cluster	STE1	1.69	2.45	112.0
Cluster	STE2	2.19	1.70	119.0
Partially relaxed structure (15 atoms)				
Periodic	STE1	1.68	2.41	107.2
Periodic	STE2	2.29	1.73	98.3
Cluster	STE1	2.40	1.69	111.2
Cluster	STE2	1.72	2.15	113.2
Other works				
Ref. 14		1.68	1.97	...
Ref. 16		1.693/1.672	2.45/2.032	146.1
Ref. 17		...	2.5	...

artificial rotations of SiO_4 tetrahedra. This is not surprising as it has been shown that the defect-induced relaxation in α quartz can propagate as far as 10 Å or more from the defect site.[41,63] Such relaxation, when modelled using the periodic supercell approach, can be inadequately reproduced if the size of the supercell is not sufficiently large. In our case, the size of the embedded QM cluster alone is ∼12 Å, which is larger than the linear size of the 72 atom supercell used to model STE.

The geometric parameters of STE calculated in this work are compared with the results of earlier calculations[9,14,16,17] in Table II. Reference 16 reports two structures obtained by optimizing two nine-atom clusters of different shapes using the Hartree-Fock method. The elongation of the Si–O distance obtained there for STE1 is similar to our results (the STE2 state is not described). Reference 17 reports several structures, however, only one of them (labeled STE-A) is thought to be responsible for the 2.5–2.7 eV luminescence bands. The geometrical structure of this STE configuration is similar to our STE1 structure. The STE configuration found in Ref. 14 using the GW method in a 18-atom periodic supercell is slightly different from our calculations. In particular, the Si atom of the broken Si–O bond adopts the sp^2 configuration and is displaced into the plane of the three oxygen atoms attached to it. However, in our case, this Si atom remains outside the plane. This comparison demonstrates qualitative agreement of the STE1 models obtained in different calculations of α-quartz and β-cristobalite.[39] However, the details of the STE structure strongly depend on the supercell or cluster size.

To investigate the dependence of the exciton properties on the size of the region in which the STE-induced relaxation is accounted for, we used the following approach. In the $Si_8O_{25}Si^*_{18}$, QM cluster embedded in the rest of the classical lattice as described above, we considered the STE relaxation within five successively expanding regions (see the top panel in Fig. 3). The smallest region includes the central O and its Si neighbors only (OSi_2), while the four other regions are constructed by adding sequentially the shells of six O atoms

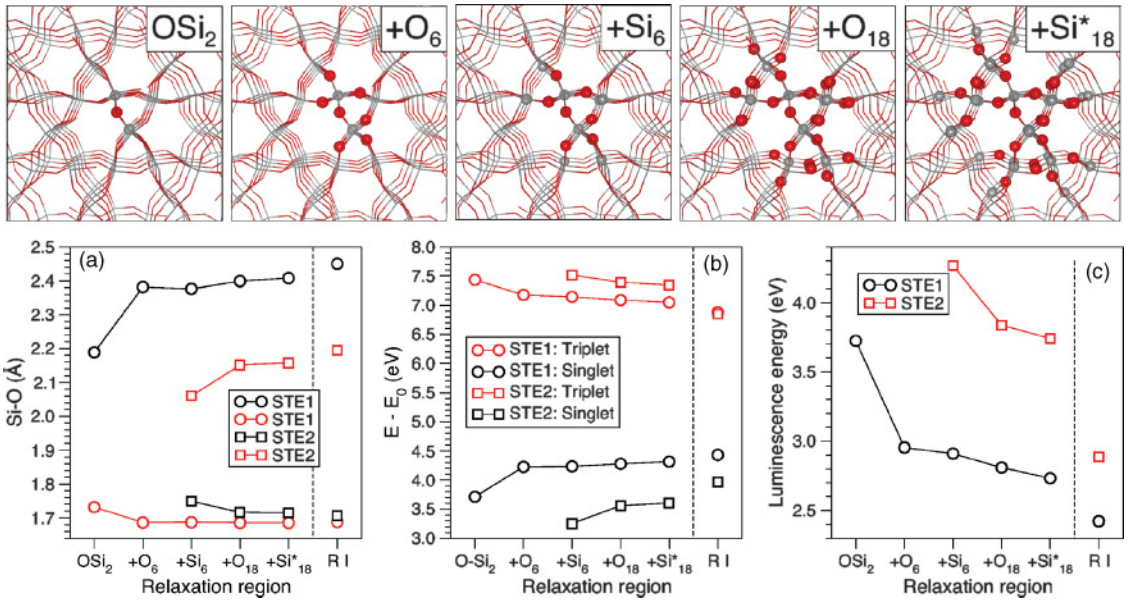

FIG. 3. (Color online) Properties of self-trapped excitons in α-quartz calculated using embedded cluster approach for several relaxation regions. Top panel shows the fully relaxed regions, shown with spheres, superimposed on the fixed lattice, shown with sticks only. Bottom panels show the calculated properties: (a) lengths of the broken and nonbroken Si-O bonds at the STEs sites, (b) STE potential energy surfaces, and (c) luminescence energies.

($+O_6$), six Si atoms ($+Si_6$), 18 O atoms ($+O_{18}$), and 18 interface Si* pseudoatoms ($+Si^*_{18}$). All other QM and classical atoms were fixed in their perfect lattice sites and only O-atom shells were allowed to relax after the system was excited into the triplet state. The results of these constrained STE calculations are summarized and compared with the results obtained for the fully relaxed excitons in Figs. 3(a)–3(c) and Table II.

The dependence of the Si-O distances at the exciton site on the size of the relaxed region is shown in Fig. 3(a). In both STE1 and STE2 states, the length of the Si-O bond does not change as long as O-Si_2-O_6 atoms are allowed to relax near the exciton site. The length of the broken Si-O bond is sensitive to both the local and medium-range atomic structures and converges slowly with increasing the size of the relaxation region.

Figure 3(b) shows the total energies of the relaxed triplet and the corresponding ground-state singlet states for partially and fully relaxed STEs calculated with respect to the total energy of the ground state (E_0). The triplet state of STE2 is always higher than that of STE1 except for the case of the fully relaxed configurations. Importantly, the triplet state of STE2 is unstable if the relaxation is confined to the O-Si_2-O_6 region only. Moreover, for the relaxation region including O-Si_2-O_6-Si_6-O_{18} atoms, the barrier for the transition from STE2 to STE1 is only 0.35 eV, while the reverse STE1-to-STE2 barrier is ~0.7 eV. These results explain quantitative differences between the results of different calculations of STE geometry and suggest that even bigger discrepancies can be expected in calculated spectroscopic properties.

2. *Properties of STE in α quartz*

The triplet exciton in α quartz (as well as in other oxides discussed below) induces localized states in the band gap and quasilocal electronic states in the valence and conduction bands of the crystal. Some of these states, pertinent to further discussion of optical transitions, are shown schematically in Fig. 4. In particular, the periodic calculations demonstrate that STE1 induces three localized levels in the gap. The electronic component of the STE1 (state A) is represented by the occupied spin-up state, formed by a $3sp$ hybrid of Si1, while its hole component (state B) is represented by an unoccupied spin-down state split from the valence band maximum (VBM) and dominated by the O1 $2p$ states (see Fig. 4 and Table III). The third state, split by 3.4 eV from the conduction band minimum (CBM), is an unoccupied spin-down state with contributions of the $3s$ and $3p$ states

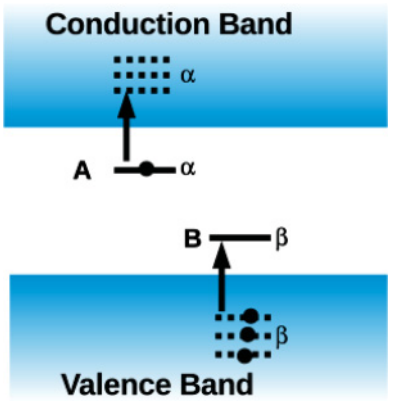

FIG. 4. (Color online) Schematic of the exciton-induced spin-up (α) and spin-down (β) localized states. States A and B correspond to the electron and the hole components of an exciton localized on a cation and an oxygen atom, respectively. Dashed lines indicate resonant exciton-induced quasilocal states inside the bands. Arrows show optical transitions between the localized states in the gap and the resonant states.

TABLE III. Splitting Δ (eV) of the exciton one-electron energy levels A and B (see Fig. 4) from the conduction and the valence band edges, respectively. Values δ (eV) show dispersion for each state.

		States A			States B		
		Δ	δ	Atom	Δ	δ	Atom
SiO_2	STE1	5.4	<0.05	Si(3*sp*)	3.0	0.05	O(2*p*)
SiO_2	STE2	5.0	<0.05	Si(3*sp*)	3.0	0.05	O(2*p*)
m-HfO_2		0.9	0.06	Hf(5*d*)	1.4	<0.05	O(2*p*)
t-HfO_2		0.9	0.1	Hf(5*d*)	2.6	0.2	O(2*p*)
c-HfO_2		0.7	0.1	Hf(5*d*)	2.4	0.3	O(2*p*)
$HfSiO_4$	STE-Hf	0.6	0.05	Hf(5*d*)	0.4	0.2	O(2*p*)
$HfSiO_4$	STE-Si	2.8	0.3	Si(3*sp*)	1.9	0.1	O(2*p*)

of Si1, which is induced by the lattice distortion. In addition, the second spin-up state of the triplet is localized on O1 and is situated inside the VB. We note that the small dispersion of these states indicates weak interaction between periodically translated excitons.

The excitation, relaxation, and photoluminescence energies corresponding to this STE are summarized in Table IV. The triplet luminescence energy obtained for this configuration is about 2.0 eV, which is smaller than the lowest experimental PL energy of 2.5 eV. This value is broadly in agreement with those obtained in previous works, which cite values between 2 and 3 eV for the luminescence energy of α-quartz.[14,17]

For STE2, the A and B states have similar character and dispersion to those induced by STE1, but appear at slightly different energies, as seen in Table III. The third state in the gap is an unoccupied spin-down state again induced by the lattice distortion. It is localized on the 3*s* and 3*p* states of Si2 and is split by only 1.5 eV from CBM. The calculated luminescence energy is 2.5 eV, i.e., larger than that in the STE1 case and similar to the lowest experimental PL energy.

The differences between the geometrical structures of STEs in the periodic and cluster models result in different PL energies: the E_l values obtained using the ΔSCF method and the embedded cluster approach are 2.4 eV for the STE1 and 2.9 eV for the STE2. This is not surprising as the calculated PL energies are rather sensitive to the size of the relaxed region [see Fig. 3(c)], which suggests that supercells exceeding the 3 × 3 × 3 extensions of the unit cell are needed in order to accurately account for this exciton-induced relaxation.

TABLE IV. Excitation (E_e), relaxation (E_r), and photoluminescence (E_l) energies and one-electron band gaps (E_g) obtained using the periodic approach and the ΔSCF method. The experimental luminescence energies ($E_{l,\mathrm{exp}}$) and band gaps ($E_{g,\mathrm{exp}}$) are provided, where possible. All energies are in eV.

		E_e	E_r	E_l	$E_{l,\mathrm{exp}}$	E_g	$E_{g,\mathrm{exp}}$
SiO_2	STE1	9.51	2.84	2.01	2.5[a]	9.2	8.9[b]
SiO_2	STE2	9.51	2.54	2.46	2.7[a]	9.2	8.9[b]
m-HfO_2		6.34	0.85	4.74	4.4[c]	6.1	5.8[d]
t-HfO_2		6.27	0.90	4.0	...	6.5	...
c-HfO_2		6.34	2.28	3.20	...	5.9	...
$HfSiO_4$	STE-Hf	8.16	1.47	6.69	...	7.5	6.5–7.0[e]
$HfSiO_4$	STE-Si	8.16	1.24	4.10	...	7.5	6.5–7.0[e]

[a]References 58 and 56.
[b]Reference 52.
[c]References 18 and 19.
[d]References 48 and 49.
[e]References 50 and 51.

The PL energies can be also computed as the lowest singlet-triplet excitation energies at the geometrical configuration of the relaxed triplet exciton. According to TD-DFT,[27] such excitation energies are 2.0 eV for STE1 and 2.5 eV for STE2. By analyzing the character of these transitions we have also identified two corresponding singlet-singlet transitions, which have energies of 2.76 eV for STE1 and 3.03 eV for STE2. We then used the transition dipole components of these allowed singlet-singlet transitions to estimate the polarization of the emission with respect to the crystal lattice *c* axis as 0.55 for STE1 and–0.4 for STE2.

These results compare fairly well with the experimentally observed PL energy of 2.74 eV and polarization of 0.48 ± 0.02, as reported in Ref. 59 although the triplet luminescence energies obtained in this paper are systematically lower than the experimental values. The existence of two types of STE with different luminescence energies and polarization has been discussed in Refs. 58 and 56 and our calculations provide a possible explanation to these data.

B. Exciton in monoclinic HfO_2

The periodic calculations predict the existence of a stable triplet exciton state in m-HfO_2. According to the Mulliken population analysis, 80% of the exciton's hole component is localized on a single 3C oxygen atom (O*), while 53% of the electron component is localized on the neighboring Hf atom (Hf*), as shown in Fig. 5. In addition, two other nearby Hf atoms share approximately 20% of the electron density of the excited electron. The exciton-induced lattice distortion is much smaller than that in α quartz. The O*-Hf* bond length increases by 0.2 Å, while other O*-Hf bond lengths increase by 0.1 Å. We did not find any exciton state with the hole component localized at a 4C oxygen atom, probably due to the higher stability of the hole on the 3C oxygen atom over the hole on the 4C oxygen atom.[21]

The triplet exciton in m-HfO_2 induces two localized gap states, A and B in Fig. 4, with dispersion smaller than 0.1 eV (see Table III). The hole state B is formed mainly by the 2*p* orbitals of O*. The electron state A is dominated by

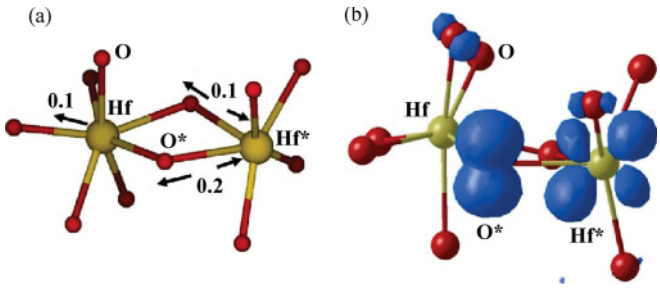

FIG. 5. (Color online) Triplet exciton in m-HfO_2: (a) exciton-induced lattice relaxation and (b) the surface of constant spin density with value S = 0.05, superimposed on the local geometrical structure. Changes of the interatomic distances are shown in Å. Bright and dark spheres represent Hf and O atoms, respectively.

5*d* states of Hf* with smaller contributions of the two other neighboring Hf atoms. The excitation energy of the triplet exciton in the perfect lattice and the luminescence energy of the relaxed exciton, calculated using ΔSCF, are 6.3 and 4.7 eV, respectively. The exciton relaxation energy in the triplet state is 0.8 eV (see also Table IV).

A similar picture emerges from the embedded cluster calculations: the band gap is larger than that in the periodic calculations by about 0.5 eV and splittings of the states B and A from their respective band edges are larger by 0.1 and 0.4 eV, respectively. Both ΔSCF method and TD-DFT put the PL energy of the STE at ∼4.8 eV.

Using TD-DFT, we have also calculated optical transitions from the valence band states to the B state of the exciton, and from the A state of the exciton to the unoccupied states in the conduction band (see Fig. 4); 20 transitions of each type have been calculated. The onset of the VBM-to-B transitions is at 0.69 eV, and the highest oscillator strength transition (at 1.29 eV) is from the oxygen ions surrounding O* to the localized hole state at O*. The onset of the A-to-CBM transitions is at 0.46 eV and the maximum oscillator strength transition (at 1.47 eV) is to a resonant state composed of 5*d* orbitals of Hf atoms surrounding the Hf* atom.

C. Excitons in tetragonal and cubic HfO_2

By analogy with the STE in m-HfO_2, we have considered several precursor configurations that were expected to favor localization of the electron and hole at neighboring Hf and O sites. However, subsequent full geometry relaxation restored the perfect lattice and a delocalized exciton state, indicating that geometrical configurations of the STEs in c- and t-HfO_2 are qualitatively different from that in m-HfO_2. Indeed, after further search, we found that in a stable STE configuration in t-HfO_2, the electron is localized by about 73% on one Hf atom (Hf*) but the hole is distributed between two oxygen atoms at the next-nearest-neighbor sites with respect to Hf*, with populations of 52% and 40%, respectively (see Fig. 6). This STE configuration stems most likely from the higher dielectric constant of the tetragonal phase (41 in our calculations), which increases the lattice polarization due to the electron and hole separation and screens the electron-hole interaction. For comparison, the dielectric constant of m-HfO_2 is only 15–25,[22,32] resulting in the stronger electron-hole attraction. The atomic displacements in this configuration are of the order of 0.1 Å, which is comparable to those in m-HfO_2, but the radius of the exciton is larger. As a result, the luminescence energy is smaller than in m-HfO_2 (see Table IV). The characteristics of the gap states A and B are similar to those found in m-HfO_2, but the B state splitting is larger than that in m-HfO_2 by 1.2 eV; it also has a slightly larger dispersion due to the interaction between more delocalized holes.

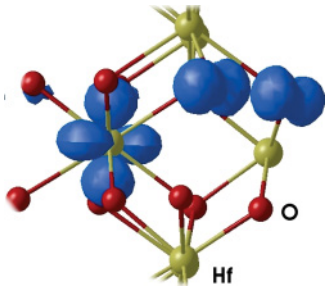

FIG. 6. (Color online) Surface of the constant spin density with value S = 0.05 calculated for the triplet STE in t-HfO_2.

In the cubic phase, the STE also self-traps, so that the hole and electron components are localized at the next-nearest-neighbor sites, with the similar Mulliken populations (73% of the electron on Hf and 42% and 50% on each oxygen). Again, a large dielectric constant, of about 31 in our calculations, may be responsible for this arrangement of the hole and the electron. The relatively large dispersion of the B state (>0.3 eV) indicates that it is more delocalized than analogous states in the m-HfO_2 and t-HfO_2. Finally, the calculated luminescence energy is the smallest among the three HfO_2 polymorphs due to the large lattice relaxation (see Table IV).

D. Excitons in $HfSiO_4$

Our calculations predict the existence of two types of self-trapped excitons in $HfSiO_4$ due to the presence of the two cation sublattices in this crystal. In one of them, denoted STE-Hf [see Figs. 7(a) and 7(c)], the electron is localized on a Hf atom (Hf*) with a Mulliken population of 86% and the hole is localized mainly on a nearest-neighbor O atom (O*) with 35% population. Approximately 12% of the hole is delocalized over three other anions bonded to a Si atom next to Hf*. The STE-induced elongation of the Hf*-O bond is ∼0.1 Å and other bonds around the Hf ion increase by 0.06 Å on average.

In the second STE, denoted STE-Si [see Figs. 7(b) and 7(d)], the electron is localized on a Si atom (Si*) and the hole is localized predominantly (94%) on one of the four surrounding O atoms (O*). As a result, the Si*-O* bond is elongated by about 0.4 Å, while the other three Si-O bonds elongate by about 0.05 Å.

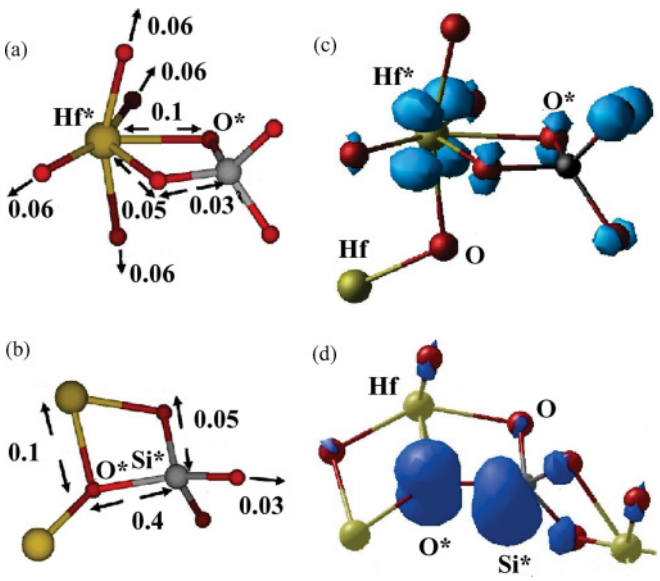

FIG. 7. (Color online) Triplet STE-Hf (top) and STE-Si (bottom) in $HfSiO_4$. (a) Lattice relaxation in STE-Hf. (b) STE-Hf surface of the constant spin density. (c) Lattice relaxation in STE-Si. (d) STE-Si constant spin density surface. Spin density value is 0.01. Changes of the interatomic distances are shown in Å. Bright, black, and dark spheres represent Hf, Si, and O atoms, respectively.

Comparison of the total energies shows that the STE-Hf is by about 0.2 eV more stable than the STE-Si. This energy difference results from two main factors. On one hand, the Hf states dominate the lower part of the conduction band, while the Si states only become predominant at about 3 eV above the CBM. However, this 3 eV difference is offset by the larger relaxation in the STE-Si.

We did not manage to obtain a solution for the perfect lattice triplet state in which the electron and the hole would be delocalized. Therefore we can only provide a lower bound for the E_e and E_l of the system. Despite underestimating the values of E_e and E_l, both of them are larger than their counterparts in m-HfO_2 (see Table IV). This is attributed to the larger band gap in this system than in any of the HfO_2 phases.

In the case of STE-Hf, the hole state (state B in Fig. 4) exhibits a larger splitting than that found for the HfO_2 polymorphs (see Table III), which is attributed to the effect of flexible SiO_4 structural elements. The splitting of the electron state (state A) is similar to that found in HfO_2 as it is dominated by the $5d$ states of Hf^*.

In the case of STE-Si, the B state is split from the VBM by a slightly lower energy than in SiO_2. Interestingly, this splitting is similar to that found for the hole state in t-HfO_2 and c-HfO_2, most likely due to the similar character of the hole redistribution over more than one oxygen atom. The electron state A has a large dispersion. Since it is formed by $3s$ and $3p$ states of Si^*, we have also calculated its splitting Δ from the Si conduction subband. The magnitude this splitting is about 6.8 eV, which is similar to the splitting of the electron level in the STE states of SiO_2 discussed above.

The presence of the two excitons in $HfSiO_4$ suggests that exciton transfer may take place between the Si and the Hf sites via an adiabatic hopping mechanism. Using the linear interpolation procedure, we found a 0.5 eV barrier energy for the transfer from the STE-Si to the STE-Hf, and 0.7 eV for the opposite process. These barriers are not as large as the ones found in quartz due to the smaller extent of the lattice relaxation induced by the $HfSiO_4$ excitons.

The $2 \times 1 \times 1$ supercell of $HfSiO_4$ used in these calculations provides a separation of only 6.0 Å between STEs in the c direction. In order to examine whether using this relatively small supercell could induce any artefacts, we calculated the STE-Hf state in a $2 \times 2 \times 2$ supercell including 192 atoms and found the same character of spin localization and lattice relaxation for the exciton state. This suggests that the $2 \times 1 \times 1$ supercell is sufficient for calculations of the $HfSiO_4$ STE states.

V. CONCLUSIONS

We used periodic and embedded cluster DFT calculations and the nonlocal density functional B3LYP to study the structure and properties of triplet excitons in α-quartz, HfO_2, and $HfSiO_4$. Unlike in previous calculations, we obtained two configurations for the triplet STE in α quartz corresponding to breaking the so-called short and long Si-O bonds. Both configurations induce large lattice distortions in the vicinity of the exciton. We demonstrate that this distortion strongly affects the electronic structure of the STE and its photoluminescence energy and cannot be treated properly in relatively small (less than 72 atoms) periodic cells and clusters. The calculated luminescence energies are broadly similar to the published experimental values.

We predict the existence of self-trapped triplet exciton states in HfO_2 and $HfSiO_4$. The character of the hole and electron localization in HfO_2 strongly depends on the symmetry and the dielectric properties of the lattice. In the monoclinic phase having the lower dielectric constants, the hole and the electron are localized predominantly on a single three-coordinated oxygen and the nearest-neighbor single hafnium atom, respectively. In the tetragonal and cubic phases, the hole is distributed over the two nearest-neighbor oxygen atoms, while the electron is localized on one hafnium atom at a next-nearest-neighbor site with respect to the hole. The STE luminescence energy predicted in m-HfO_2 is close to that attributed to STE in experimental studies,[18,19] which lends some support to the existence of the STE in this material.

For $HfSiO_4$, we predict the existence of two different triplet STE configurations with two distinct luminescence energies. In one of them, the electron is localized on an Hf atom, whereas the hole is delocalized over the four oxygen atoms. In the other one, the electron is localized on a Si atom whereas the hole is strongly localized on the nearest-neighbor O atom.

It is interesting to note the charge transfer character of all STE models obtained in this work. The models and photoluminescence energies predicted for $HfSiO_4$ are in a qualitative and even semiquantitative agreement with those discussed for triplet STE in Be_2SiO_4 and more complex silicates in Ref. 4. More generally, these results shed light on the processes and models of localization of electronic excitations in low-symmetry complex oxides with different structures and dielectric constants, which have been discussed recently in the context of new scintillators as well as microelectronic devices.[4,23,64,65]

ACKNOWLEDGMENTS

P.V.S. is grateful to the Royal Society for financial support. D.M.R. was supported by the EPSRC Grant No. GR/S80080/01 and NERC Grant No. NE/F017871/1. Computer time on the Hector facility was provided to the Materials Chemistry Consortium under EPSRC-GB Grant No. GR/S13422/01 "Materials Chemistry using Teraflop Computing." The authors acknowledge the use of the UCL Legion High Performance Computing Facility and associated support services in the completion of this work.

[1] R. T. Song and R. T. Williams, *Self-Trapped Excitons* (Springer-Verlag, Berlin Heidelberg New York, 1993).

[2] A. M. Stoneham and N. Itoh, *Materials Modification by Electronic Excitation* (Cambridge University Press, Cambridge, 2000).

[3] A. Lushchik, M. Kirm, C. Lushchik, I. Martinson, and G. Zimmerer, J. Lumin. **87-89**, 232 (2000).

[4] V. Ivanov, A. Kikas, T. Käämbre, M. Kirm, I. Kuusik, and V. Pustovarov, IOP Conf. Series: Materials Science and Engineering **15**, 012088 (2010).

[5]M. Ueta, H. Kanzaki, K. Kobayashi, Y. Toyozawa, and E. Hanamura, *Excitonic Processes in Solids* (Springer-Verlag, Berlin, 1986)
[6]A. Sumi, J. Phys. Soc. Jpn. **43**, 1286 (1977).
[7]A. L. Shluger, A. H. Harker, V. E. Puchin, N. Itoh, and C. R. A. Catlow, Model. Simul. Mater. Sc. **1**, 673 (1993).
[8]A. L. Shluger and K. Tanimura, Phys. Rev. B **61**, 5392 (2000).
[9]A. J. Fisher, W. Hayes, and A. M. Stoneham, J. Phys. Condens. Matter **2**, 6707 (1990).
[10]V. E. Puchin, A. L. Shluger, and N. Itoh, Phys. Rev. B **52**, 6254 (1995).
[11]J. L. Gavartin, P. V. Sushko, and A. L. Shluger, Phys. Rev. B **67**, 035108 (2003).
[12]A. L. Shluger, K. P. McKenna, P. V. Sushko, D. Muñoz Ramo, and A. V. Kimmel, Model. Simul. Mater. Sc. **17**, 084004 (2009).
[13]S. Lany and A. Zunger, Phys. Rev. B **80**, 085202 (2009).
[14]S. Ismail-Beigi and S. G. Louie, Phys. Rev. Lett. **95**, 156401 (2005).
[15]Y. Ma and M. Rohlfing, Phys. Rev. B **75**, 205114 (2007).
[16]A. J. Fisher, W. Hayes, and A. M. Stoneham, Phys. Rev. Lett. **64**, 2667 (1990).
[17]R. M. Van Ginhoven, H. Jónsson, K. A. Peterson, M. Dupuis, and L. R. Corrales, J. Chem. Phys. **118**, 6582 (2003).
[18]J. Aarik, H. Mändar, M. Kirm, and L. Pung, Thin Solid Films **466**, 41 (2004).
[19]M. Kirm, J. Aarik, M. Jürgens, and I. Sildos, Nucl. Instr. Meth. A **537**, 251 (2005).
[20]J.-W. Park, D.-K. Lim, H. Lee, and S.-H. Choi, J. Appl. Phys. **104**, 033521 (2008).
[21]D. Muñoz Ramo, A. L. Shluger, J. L. Gavartin, and G. Bersuker, Phys. Rev. Lett. **99**, 155504 (2007).
[22]X. Zhao and D. Vanderbilt, Phys. Rev. B **65**, 233106 (2002).
[23]A. F. Zatsepin, A. I. Kukharenko, V. A. Pustovarov, V. Y. Yakovlev, and S. O. Cholakh, Phys. Solid State **51**, 465 (2009).
[24]S. Albrecht, G. Onida, and L. Reining, Phys. Rev. B **55**, 10278 (1997).
[25]A. V. Kimmel, P. V. Sushko, and A. L. Shluger, J. Non-Cryst. Solids **353**, 599 (2007).
[26]S. Sicolo, G. Palma, C. Di Valentin, and G. Pacchioni, Phys. Rev. B **76**, 075121 (2007).
[27]M. J. Frisch *et al.*, GAUSSIAN 03 Revision C02 (Gaussian, Wallingford, CT, 2003).
[28]R. Dovesi, V. Saunders, C. Roetti, R. Orlando, C. M. Zicovich-Wilson, F. Pascale, B. Civalleri, K. Doll, N. M. Harrison, I. J. Bush, P. D'Arco, and M. Llunell, CRYSTAL06: User's Manual (University of Torino, 2006).
[29]A. D. Becke, J. Chem. Phys. **98**, 5648 (1993).
[30]C. Lee, W. Yang, and R. G. Parr, Phys. Rev. B **37**, 785 (1988).
[31]D. Muñoz Ramo, J. L. Gavartin, A. L. Shluger, and G. Bersuker, Phys. Rev. B **75**, 205336 (2007).
[32]D. Muñoz Ramo, A. L. Shluger, and G. Bersuker, Phys. Rev. B **79**, 035306 (2009).
[33]P. V. Sushko, S. Mukhopadhyay, A. S. Mysovsky, V. B. Sulimov, A. Taga, and A. L. Shluger, J. Phys. Condens. Matter **17**, S2115 (2005).
[34]L. Giordano, P. V. Sushko, G. Pacchioni, and A. L. Shluger, Phys. Rev. B **75**, 024109 (2007).
[35]L. Giordano, P. V. Sushko, G. Pacchioni, and A. L. Shluger, Phys. Rev. Lett. **99**, 136801 (2007).
[36]F. Cora, M. Alfredsson, G. Mallia, D. S. Middlemiss, W. C. Mackrodt, R. Dovesi, and R. Orlando, Struct. Bond. **113**, 171 (2004).
[37]P. V. Sushko, A. L. Shluger, M. Hirano, and H. Hosono, J. Am. Chem. Soc. **129**, 942 (2007).
[38]W. J. Stevens, M. Krauss, H. Basch, and P. G. Jasien, Can. J. Chem. **70**, 612 (1992).
[39]A. L. Shluger and E. V. Stefanovich, Phys. Rev. B **42**, 9664 (1990).
[40]J. L. Gavartin and A. L. Shluger, Phys. Rev. B **64**, 245111 (2001).
[41]V. B. Sulimov, P. V. Sushko, A. H. Edwards, A. L. Shluger, and A. M. Stoneham, Phys. Rev. B **66**, 024108 (2002).
[42]I. V. Abarenkov, Phys. Rev. B **76**, 165127 (2007).
[43]B. W. H. van Beest, G. J. Kramer, and R. A. van Santen, Phys. Rev. Lett. **64**, 1955 (1990).
[44]P. J. Hay and W. R. Wadt, J. Chem. Phys. **82**, 270 (1985).
[45]E. Gnani, S. Reggiani, R. Colle, and M. Rudan, IEEE Trans. Electron Devices **47**, 1795 (2000).
[46]A. L. Shluger, A. S. Foster, J. L. Gavartin, and P. V. Sushko, in *In Nano and Giga Challenges in Microelectronics*, edited by J. Greer, A. Korkin, and J. Labanowski (Elsevier, 2003), pp. 151–222.
[47]K. Xiong, Y. Du, K. Tse, and J. Robertson, J. App. Phys. **101**, 024101 (2007).
[48]N. V. Nguyen, A. V. Davydov, D. Chandler-Horowitz, and M. M. Frank, Appl. Phys. Lett. **87**, 192903 (2005).
[49]*High-k Dielectrics*, edited by M. Houssa (IOP Publishing, Bristol and Philadelphia, 2004) p. 597.
[50]H. Kato, T. Nango, T. Miyagawa, T. Katagiri, K. S. Seol, and Y. Ohki, J. Appl. Phys. **92**, 1106 (2002).
[51]G. B. Rayner, D. Kang, Y. Zhang, and G. Lucovsky, J. Vac. Sci. Technol. B **20**, 1748 (2002).
[52]A. C. Wright, in *Defects in SiO_2 and Related Dielectrics*, edited by G. Pacchioni, L. Skuja, and D. L. Griscom, Science and Technology NATO Science Series, Series II: Mathematical and Physical Chemistry (Kluwer, Dordrecht, 2000).
[53]L. Levien, C. T. Previtt, and D. J. Weidner, J. Mater. Sci. **27**, 5397 (1992).
[54]L. Levien, C. T. Previtt, and D. J. Weidner, Am. Mineral **65**, 920 (1980).
[55]J. A. Speer and B. J. Cooper, Am. Mineral. **67**, 804 (1982).
[56]A. N. Trukhin, M. Kink, Y. Maksimov, and R. Kink, Solid State Commun. **127**, 655 (2003).
[57]A. N. Trukhin and A. E. Plaudis, Sov. Sol. St. Phys. **21**, 1109 (1979).
[58]A. N. Trukhin, Nucl. Instrum. Meth. B **334**, 91 (1994).
[59]K. Tanimura and L. E. Halliburton, Phys. Rev. B **34**, 2933 (1986).
[60]A. L. Shluger, J. Phys. C: Solid State Phys. **21**, L431 (1988).
[61]R. M. Van Ginhoven, H. Jónsson, and L. R. Corrales, J. Non-Cryst. Sol. **352**, 2589 (2006).
[62]See Supplemental Material at http://link.aps.org/supplemental/10.1103/PhysRevB.85.024120 for movies of the lattice relaxation of STE1 and STE2 in periodic and cluster models.
[63]A. S. Mysovsky, P. V. Sushko, S. Mukhopadhyay, A. H. Edwards, and A. L. Shluger, Phys. Rev. B **69**, 085202 (2004).
[64]V. Y. Ivanov, E. S. Shlygin, V. A. Pustovarov, V. V. Mazurenko, and B. V. Shul'gin, Phys. Solid State **50**, 1692 (2008).
[65]M. Nikl, V. V. Laguta, and A. Vedda, Phys. Status Solidi B **245**, 1701 (2008).